ELSEVIER

Journal of Molecular Structure 509 (1999) 237–254

Journal of
MOLECULAR
STRUCTURE

www.elsevier.nl/locate/molstruc

1,1,2-Triiododisilane ($I_2HSi–SiH_2I$): molecular structure, internal rotation and vibrational properties determined by gas-phase electron diffraction, infrared and Raman spectroscopy, and ab initio molecular orbital- and density functional calculations ☆

T.H. Johansen[a,*], K. Hagen[a], K. Hassler[b], G. Tekautz[b], R. Stølevik[a]

[a]*Department of Chemistry, Norwegian University of Science and Technology, NTNU, N-7491 Trondheim, Norway*
[b]*Institut für Anorganische Chemie, Technische Universität, Stremayrgasse 16, A-8010 Graz, Austria*

Received 18 March 1999; accepted 6 April 1999

Abstract

The molecular structure, internal rotation and vibrational properties of 1,1,2-triiododisilane (TIDS), $I_2HSi–SiH_2I$, have been studied using gas phase electron diffraction (GED) data at an average temperature of 52°C, together with infrared and Raman spectroscopy, and ab initio molecular orbital- and density functional calculations. The title compound exists in the gas and liquid phases as a mixture of two minimum conformers, *anti*, with a torsional angle ϕ(HSiSiI) = 180°, and *gauche*, with a torsional angle ϕ(HSiSiI) ≈ 80°. Discrepancies were found between the experimental results and the theoretical calculations regarding conformational stability. The GED analysis, using a cosine potential function in describing the torsional motion, gives about 51% contribution of the *anti* conformer, while the corresponding spectroscopic result contributes about 64%. The theoretical calculations give the *gauche* conformer a lower energy of average value 1.1 kcal mol^{-1}, corresponding to 90% of this conformer in the gaseous mixture. Some structural parameter values obtained from the GED refinements, using results from the theoretical calculations as constraints, are as follows (torsional vibrational average values with estimated 2σ uncertainties): Bond lengths (r_g): r(Si–Si) = 2.329(12) Å, r(Si–I) = 2.449(3) Å (average value of the three Si–I bonds), r(Si–H) = 1.527 Å (estimated value). Bond angles ($\angle_\alpha$): ∠(SiSiI) = 109.9(4)° (average value), ∠ISiI = 110.5(4)°, ∠ISiH = 109.0(2)°. The torsional cosine potential-function parameters V_1, V_2 and V_3 were obtained from the GED data analysis. Vibrational spectra were presented and analysed, aided by normal coordinate calculations and ab initio results.

Keywords: 1,1,2-Triiododisilane; Torsional potential function; Gas electron diffraction; Vibrational spectroscopy

1. Introduction

The study of the molecular structure, conformation and torsional potential of halogenated disilanes poses many different challenges. We recently reported an experimental molecular structure and torsional potential function for 1,1,2,2-tetrachlorodisilane ($Cl_2HSi–SiHCl_2$) [1] using gas-phase electron diffraction (GED) data, aided by previous results from an IR and Raman vibrational spectroscopic study [2]. It is well known that the torsional barrier heights in silane compounds are lower than in the corresponding

☆ Dedicated to Professor Peter Klæboe on the occasion of his 70th birthday.

* Corresponding author. Tel.: + 47-73-590752; fax: + 47-73-596255.

E-mail address: torjoh@alfa.itea.ntnu.no (T.H. Johansen)

0022-2860/99/$ - see front matter
PII: S0022-2860(99)00224-0

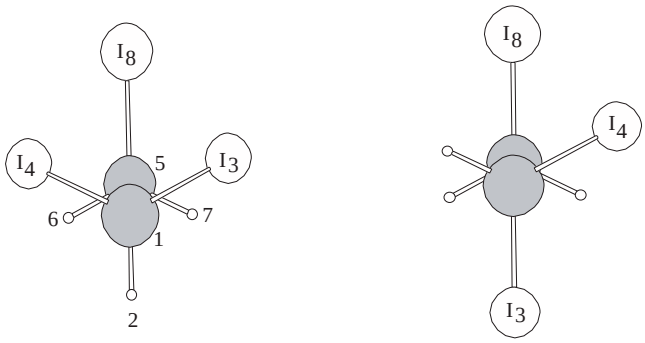

Fig. 1. Molecular models of *anti* and *gauche* conformers of 1,1,2-triiododisilane (TIDS) showing the atom numbering.

alkanes [3]. This experimental fact manifested itself in that an appropriate torsional potential function, as well as a scaled quantum-mechanical (SQM) force field, appeared necessary in several GED studies on silane type molecules [1,4–6], using the dynamic model approach. For the persubstituted disilane molecules, $X_3Si–SiX_3$, with X = H, F, Cl and CH_3, the determination of the rotational barrier heights have especially been given attention, both experimentally as reviewed by Oberhammer [6], and more recently by ab initio molecular orbital (MO) and density functional theory (DFT) calculations [3,7].

Experimental geometries for iodosilanes are very scarce. GED studies on the 1,2-di- and 1,1,2,2-tetraiododisilanes were reported by Røhmen et al. in 1991 [8], and a microwave study on iododisilane ($IH_2Si–SiH_3$) was reported in 1982 by Durig et al. [9]. Also, the solid state X-ray structure of hexaiododisilane ($I_3Si–SiI_3$) was reported in 1996 [10]. To our knowledge, these are the only experimental studies on molecular geometry that exist for iododisilane compounds. The experimental difficulties in investigating iododisilanes are quite clear, as they have been reported to be thermally unstable, and to react vigorously with air and moisture [11]. Theoretically, there is always the challenge of describing the iodine atoms by ab initio quantum mechanical methods. There are not many all-electron or valence-electron basis sets in consistent use for the iodine atom, but a widely accepted set based on ab initio effective core potentials (ECP), including relativistic effects, was reported by Wadt and Hay in 1985 [12]. Their ECP representations were also incorporated into standard GAUSSIAN 94 [13] basis sets such as LanL2DZ and LanL2MB ("Los Alamos ECP"; we will abbreviate this as HW–ECP). The ECP basis sets of Stephens, Basch and Krauss (SBK) [14,15] have also been incorporated into GAUSSIAN 94, and into the GAMESS software package [16]. The most readily available all-electron basis set in common use for the iodine atom is the 3-21G* set, but in the GAUSSIAN 94 implementation, the polarization function applies to second row atoms only (Na–Cl) [17]. In the work presented in this paper, we combined the ECP-based iodine representations with Hartree–Fock (HF), Møller–Plesset (MP2) and density functional theory (DFT), using both the SBK and HW–ECP basis sets. The DFT theories applied were Becke's hybrid exchange functional (B3) combined with both the Lee–Yang–Parr (LYP) and the Perdew–Wang (PW91) correlation functionals (B3LYP and B3PW91) [18].

The experimental and theoretical findings for the molecule 1,1,2-triiododisilane ($I_2HSi–SiH_2I$; Fig. 1) will be described in this paper, using the GED data, IR- and variable temperature Raman spectroscopy, and ab initio MO and DFT calculations.

2. Experimental

2.1. Synthesis and vibrational spectroscopy

General: As iodosilanes are easily attacked by oxygen and moisture, all manipulations were carried out under an atmosphere of dry nitrogen. All solvents

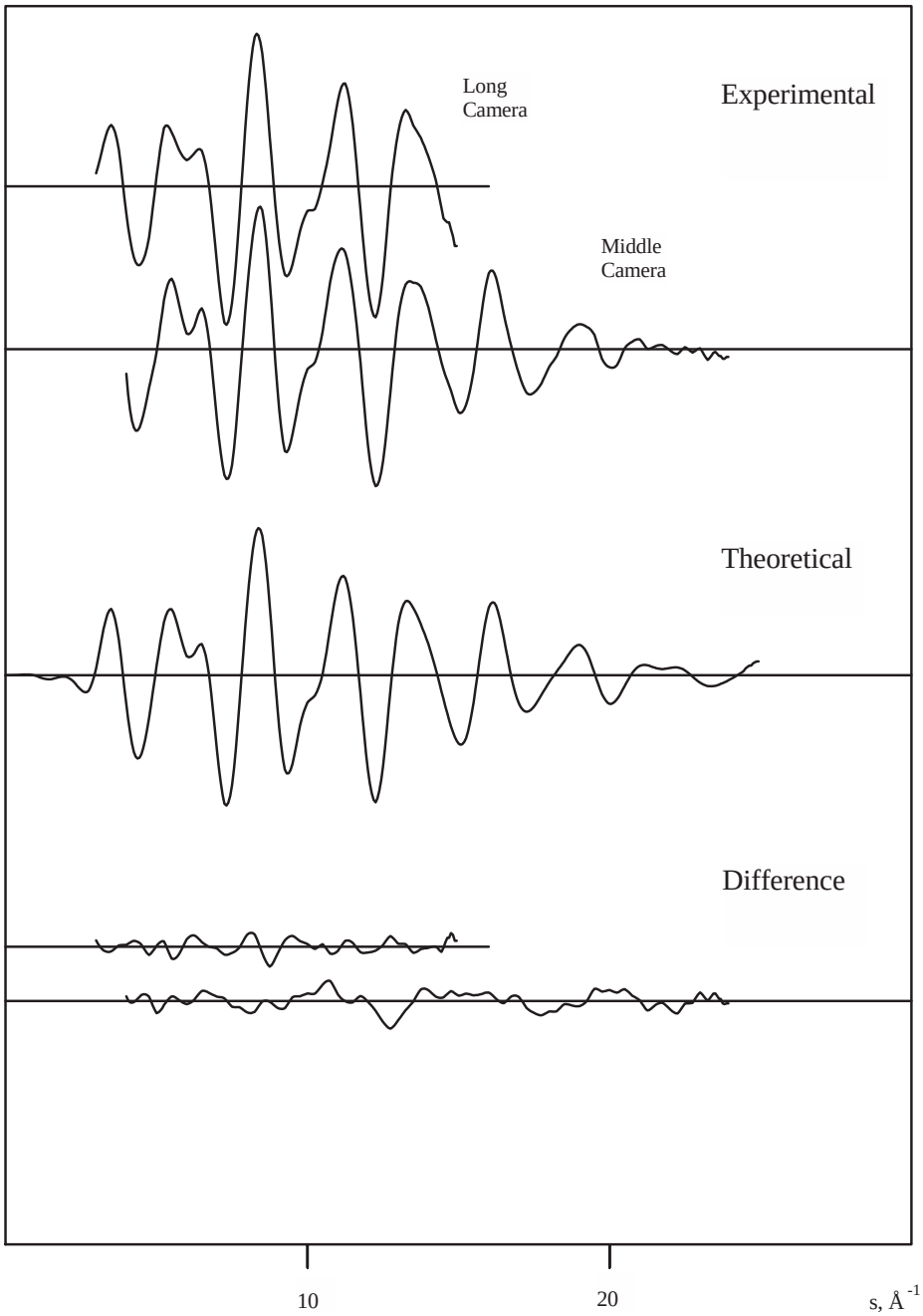

Fig. 2. Intensity curves ($sI_m(s)$) for 1,1,2-triiododisilane. The experimental curves are averages of 6(LC) + 5(MC) plates from the two camera distances. The theoretical curve was calculated from the structural parameters given in Table 5. The difference curves result from subtracting the relevant part of the theoretical curve from the experimental curves.

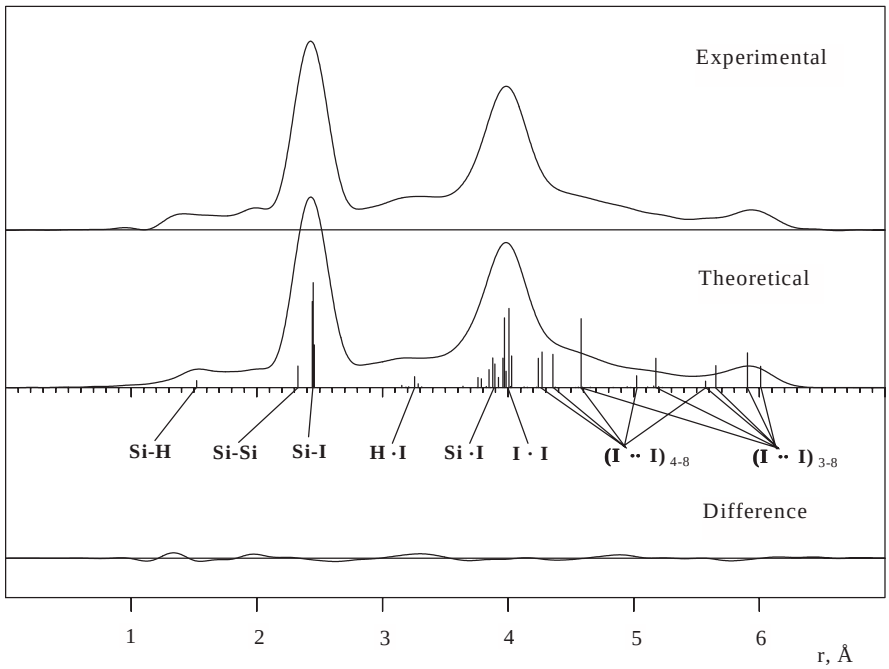

Fig. 3. Radial distribution curves for 1,1,2-triiododisilane. The experimental curve was calculated from the composite of the two average experimental curves shown in Fig. 2 with the use of theoretical data for the region $0 \leq s$ (Å^{-1}) ≤ 2.75 and $B = 0.0025$ Å^2. The difference curve is experimental minus theoretical. The vertical lines indicate the interatomic distances, they have lengths proportional to the distance weights.

were dried by refluxing over potassium and purified by distillation under an N_2-atmosphere.

Synthesis: 2.33 g (8.02 mmol) of 1,1,2-triphenyldisilane $Ph_2HSiSiH_2Ph$ (prepared from $Ph_2HSiSiHPh_2$ by treatment with one equivalent of CF_3SO_3H, followed by a reduction with $LiAlH_4$ [19]) was placed in a thick-walled glass tube, into which then was condensed a large excess of hydrogen iodide (HI, approx. 15 g). The glass tube was then sealed carefully and placed in a refrigerator at −30°C for three days (72 h). After this time, the tube was opened carefully and connected to a vacuum line. The excess of HI and all volatile products (mainly C_6H_6) were separated at a pressure of 5 mm Hg. The colourless oily residue (3.53 g, 100%) consisted of pure $I_2HSiSiH_2I$, which was purified further by fractional distillation, $Kp_2 = 92$–95°C.

Elemental analysis (calc./found): I: 86.54/86.20%

^{29}Si–NMR $I_2HSi^*SiH_2I$:

Si: $\delta = -92.4$ ppp, $^1J(SiH) = 266.3$ Hz, $^2J(SiH) = 18.3$ Hz

*Si: $\delta = -77.3$ ppp, $^1J(SiH) = 241.4$ Hz, $^2J(SiH) = 21.0$ Hz

Spectra: ^{29}Si-NMR spectra of solutions of $I_2HSiSiH_2I$ in dry C_6D_6 (30–50%) were recorded on a Bruker MSL-300 spectrometer at temperatures of 22°C. Infrared spectra of the neat liquids in the range 4000–250 cm^{-1} were recorded on a Perkin Elmer 883 spectrometer as films between CsBr-plates. Raman spectra in the range 4000–50 cm^{-1} were taken with a T 64000 triple monochromator spectrometer of Jobin Yvon. Solid (173 K) and liquid (293 K) Raman spectra were recorded. The spectra were excited with the green (514 nm) line of an Argon-laser. All samples were distilled or condensed into 1 mm capillaries, which were then sealed under a dry nitrogen atmosphere. Low temperature spectra were obtained with the help of a cryostat sporting a copper block, which could be cooled with liquid nitrogen and heated resistively. The capillary was mounted on the copper block

Table 1
Wavenumbers (cm^{-1}) of bands observed for 1,1,2-triiododisilane ($I_2HSi-SiH_2I$) (s, strong; b, broad; sh, shoulder; m, medium; w, weak; as, antisymmetric; v, very)

IR (l)	Raman (l, 293 K)	Raman (s, 173 K)	Assignment	Description
2168 sh			ν'_{12}	νSiH
2160 s	2160 vs	2160 vs	ν_1, ν_2, ν_{12}	νSiH
	916 vvw,b	912 vvw		
902 s	898 m	893 mw	ν_3	δSiH_2
855 w				
775 w	779 vw,b	775 vw	ν'_4	γSiH_2
768 ms	767 w	763 w	ν_4	γSiH_2
739 ms	736 w,b	739 vw	ν_{13}	δHSiI
712 vs	712 vw,b	707 w	ν_5	δSiSiH
675 vs	677 w	669 w	ν'_5	δSiSiH
	635 w,b	636 w	ν_{14}	τSiH_2
623 m	627 w	622 w	ν'_{14}	τSiH_2
477 w,b	479 m	476 m	ν'_6	
465 w,b	463 m	461 m	ν_6, ν_{15}	νSiSi, ρSiH_2
388 sh?			ν'_{16}	$\nu_{as}SiI_2$
383 vs	382 m	380 m	ν_{16}	$\nu_{as}SiI_2$
353 vs	353 s	350 s	ν_7	νSiI
	328 m	324 m	impurity?	
	297 vs	297 sh	ν'_8	ν_sSiI_2
	293 vs	281 vs	ν_8	ν_sSiI_2
	214 m	211m	impurity?	
	175 m	171 m	ν_{10}	δSiI_2
	128 sh	128 sh		
	123 m	120 m	ν'_{10}	δSiI_2
	102 s	100 s	ν'_{11}	δSiSiI
	90 ms	88 s	ν_9	γSiI_2
	76 m	74 m	ν_{17}, ν'_9	τSiI_2, γSiI_2

whose temperature was monitored with a thermocouple.

2.2. Gas electron diffraction

Electron-diffraction patterns were recorded with the Balzers Eldigraph KD-G2 (42 kV) at the University of Oslo [20] on Kodak Electron Image plates with an average nozzle-tip temperature of 325 K. Nominal nozzle-to-plate distances were 500 and 250 mm for the long camera (LC) and the middle camera (MC) distance experiments, respectively. The electron wavelength was $\lambda = 0.058434$ Å. Six diffraction photographs from the LC and five from the MC camera distances were used in the analysis. A voltage/distance calibration was made with benzene as reference (r_a(C = C) = 1.3975 Å) [21]. Optical densities were measured using an Agfa ARCUS II commercial scanner [22] at the University of Oslo, and the data were reduced in the usual way [23–25]. The ranges of data were $3.00 \leq s/Å^{-1} \leq 15.00$ and $4.00 \leq s/Å^{-1} \leq 24.00$ for the LC and the MC distance experiments, respectively. The data interval was $\Delta s = 0.25$ $Å^{-1}$.

A calculated background [26] was subtracted from the data for each plate to yield the experimental intensity curves in the form $sI_m(s)$. The average experimental intensity curves are shown in Fig. 2. In Fig. 3 is shown the final experimental radial distribution (RD) curve calculated in the usual way from the modified molecular intensity curve $I'(s) = sI_m(s)Z_lZ_l(A_lA_l)^{-1}\exp(-0.0025s^2)$, where $A = s^2F$ and F is the absolute value of the complex electron scattering amplitudes. Theoretical intensity data were used for $s \leq 2.75$ $Å^{-1}$ in the experimental curve before the RD curve was calculated. The scattering amplitudes and phases were taken from the tables in Ref. [27].

Table 2
Symmetry coordinates (not normalized) used in the normal coordinate analysis of 1,1,2-triiododisilane ($I_2HSi–SiH_2I$)

Species	No.	Description	Symmetry coordinate
A′	S_1	νSiH	u_4
	S_2	ν_sSiH$_2$	$u_5 + u_6$
	S_3	δSiH$_2$	$4\delta - \beta_5 - \beta_6 - \gamma_5 - \gamma_6$
	S_4	γSiH$_2$	$\beta_5 + \beta_6 - \gamma_5 - \gamma_6$
	S_5	δSiSiH	$5\beta_4 - \alpha_1 - \alpha_2 - \gamma_1 - \gamma_2 - \varphi$
	S_6	νSiSi	R
	S_7	νSiI	s_3
	S_8	ν_sSiI$_2$	$s_1 + s_2$
	S_9	γSiI$_2$	$\alpha_1 + \alpha_2 - \gamma_1 - \gamma_2$
	S_{10}	δSiI$_2$	$4\varphi - \alpha_1 - \alpha_2 - \gamma_1 - \gamma_2$
	S_{11}	δSiSiI	$5\alpha_3 - \beta_5 - \beta_6 - \gamma_5 - \gamma_6 - \delta$
A″	S_{12}	ν_{as}SiH$_2$	$u_5 - u_6$
	S_{13}	δHSiI	$\alpha_1 - \alpha_2 + \gamma_1 - \gamma_2$
	S_{14}	τSiH$_2$	$\beta_5 - \beta_6 - \gamma_5 + \gamma_6$
	S_{15}	ρSiH$_2$	$\beta_5 - \beta_6 + \gamma_5 - \gamma_6$
	S_{16}	ν_{as}SiI$_2$	$s_1 - s_2$
	S_{17}	τSiI$_2$	$\alpha_1 - \alpha_2 - \gamma_1 + \gamma_2$
	S_{18}	SiSi-torsion	$\sum\tau_i$

3. Structure analysis

3.1. Ab initio molecular orbital and density functional theory calculations

3.1.1. Constraints in the GED study

Ab initio MO and DFT calculations were used to establish the constraints in our dynamic GED model by incorporating the calculated geometrical differences between seven pseudo-conformers as constants in the refinements. The geometries for both the stable conformers of TIDS were fully optimized using GAUSSIAN 94 [13] and GAMESS [16], and the following combinations of methods/basis sets: HF/3-21G, HF/SBK–ECP (with a valence double-zeta basis and a single set of polarization function on all atoms), MP2/SBK–ECP, HF/6-31G(d)/HW–ECP(I) (6-31G(d) for Si and H, HW–ECP for I), B3PW91/LanL2DZ, B3LYP/3-21G and finally B3LYP/3-21G*. Geometry optimizations were also performed at the B3LYP/3-21G* level for each pseudo-form at 30° interval, and these results were used as constraints in the refinement. The procedure of using ab initio results as constraints in the GED analysis is now well established [28–30].

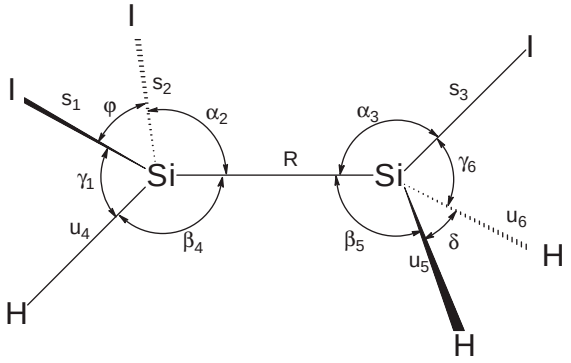

Fig. 4. Notation of the internal coordinates used for the construction of symmetry coordinates.

3.1.2. Zero-point energies

Zero-point vibrational energies (ZPE) were also estimated at several of the aforementioned ab initio optimized geometries. The ZPE's were all found to be higher in the *gauche* conformer, and the values for the ZPE differences varied from 0.0025 kcal mol^{-1} (HF/6-31G(d)/HW–ECP(I)) to 0.0301 kcal mol^{-1} (B3LYP/3-21G). Calculated entropies at the latter level were deemed unreasonable, and a basis-set of at least 6-31G(d) quality should normally be used for thermodynamic considerations. Energy estimates obtained for the pseudo-conformers at the B3LYP/3-21G* level were used to calculate the theoretical pseudo-conformational composition, by using simple Boltzmann statistics.

3.2. Vibrational spectroscopy

3.2.1. Vibrational spectra

The wavenumbers of the bands observed in the IR- and Raman spectra of liquid TIDS are summarized in Table 1. Raman shifts for the solid (173 K) are also presented. The numbering and description of the modes as given in the column 'assignment' follows from the definition of the symmetry coordinates which is presented in Table 2 and Fig. 4. Primed modes refer to the *gauche* conformer whenever a resolvable frequency difference between the conformers could be observed, while the unprimed refers to the *anti* conformer. The Raman spectrum in the range 40–900 cm^{-1} is presented in Fig. 5, and an enlarged portion in the range 90–400 cm^{-1} in Fig. 6. The spectra are interpreted qualitatively making use of

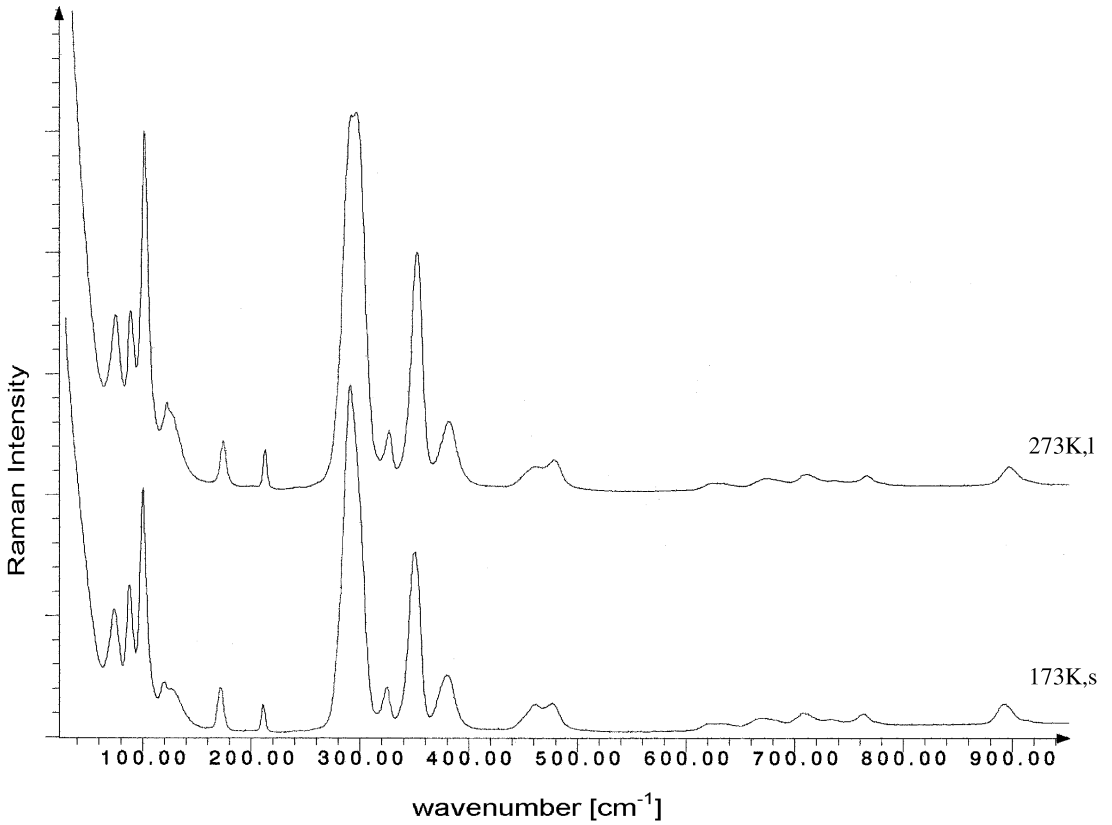

Fig. 5. Raman spectra of liquid and solid 1,1,2-triiodosilane in the range 40–900 cm^{-1}.

the concept of group vibrations. They can be divided into the range for the SiH stretching modes (2160–2170 cm^{-1}), for the SiSiH and ISiH deformation modes (900–600 cm^{-1}, except ρSiH_2 which can be shifted to even lower wavenumbers), for the SiSi and SiI stretching modes (490–280 cm^{-1}) and for the heavy atom deformations (<220 cm^{-1}). Generally, SiH deformations appear as weak Raman lines but absorb strongly in the IR region.

The SiH stretching modes, ν_1, ν_2 and ν_{12}, coincide into a single non-resolvable line in the Raman spectrum. In the IR spectrum there is a shoulder at 2168 cm^{-1} which can be assigned as ν'_{12}. The SiH deformation modes, ν_3 (δSiH_2) and ν_{13} ($\delta HSiI$), show no conformational dependence. This is clearly not the case for the remaining modes γSiH_2 (ν_4, ν'_4), $\delta SiSiH$ (ν_5, ν'_5) and τSiH_2 (ν_{14}, ν'_{14}). All are split into doublets due to rotational isomerism. ρSiH_2 (ν_{15}, ν'_{15}) coincides with $\nu SiSi$ (ν_6), an assignment which is supported by the ab initio calculations. The SiH deformations are followed by the SiSi and SiI stretching modes. The modes, ν_6 and ν'_6, are clearly separated, which is not the case for the antisymmetric SiI_2 stretch ν_{16}. However, there is an indication of a shoulder in the IR spectrum, which can be assigned as ν'_{16}. The SiI stretch ν_7 is totally insensitive against conformational impacts, but not the symmetric SiI_2 stretch ν_8. The modes ν_8 and ν'_8 appear as strong Raman bands separated by 4 cm^{-1} which we were able to resolve. The two lines at 328 and 214 cm^{-1}, which flank the ν_8 doublet, probably originate from the byproducts such as $I_2HSiSiHI_2$, which may be formed by halogen exchange reactions such as

$$2I_2HSiSiH_2I \rightarrow I_2HSiSiHI_2 + I_2HSiSiH_3 \text{ or } IH_2Si\text{-}SiH_2I$$

It is not easy to avoid such reactions, which make the storage of iododisilanes over longer periods

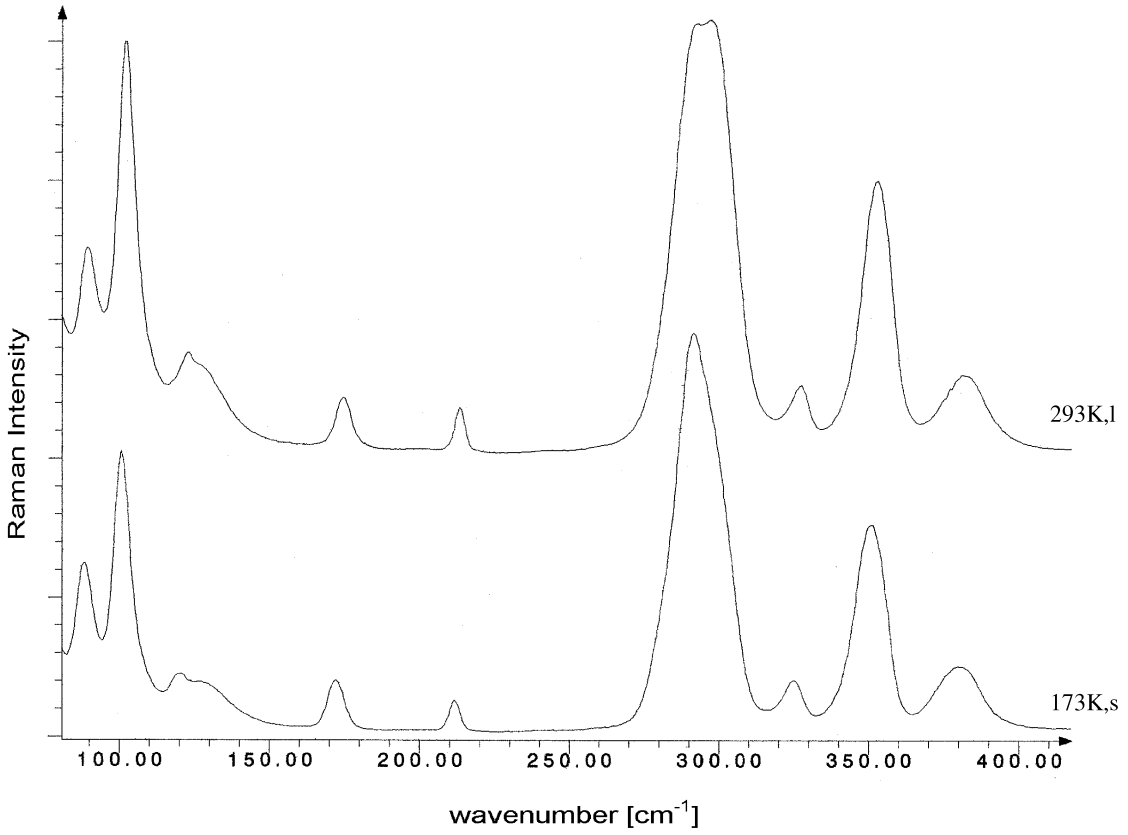

Fig. 6. Raman spectra of liquid and solid 1,1,2-triiododisilane in the range 90–400 cm^{-1}.

impossible, even at low temperatures. The deformation modes of the heavy atoms, γSiI_2 (ν_9, ν'_9) and δSiI_2 (ν_{10}, ν'_{10}) are clearly dependent on the conformation, with the difference of the wavenumbers being as large as 50 cm^{-1}. τSiI_2 (ν_{17}) is observed at 76 cm^{-1}. The SiSi-torsion and SiSiI deformation could not be observed due to their small wavenumbers. It should be noted that many of the deformation modes are heavily coupled kinetically as can be seen from the PED, which makes the description and assignment of a specific mode a more or less arbitrary task.

3.2.2. Normal coordinate analysis

The detailed assignments for the present molecule are based on the ab initio calculations using basis sets and pseudo-potentials that have been used earlier for the interpretation of the vibrational spectra of the iododisilanes $I_nH_{3-n}SiSiH_3$, with $n = 1,2,3$ [31]. The force field (Hessian matrix) defined in Cartesian coordinates was transformed into a force field defined in non-redundant symmetry coordinates, which themselves were chosen as linear combinations of (redundant) internal coordinates (cf. Table 2 for *anti* TIDS and Fig. 4). An identical set was used for the *gauche* conformer. The ab initio force fields calculated at the MP2/SBK–ECP level were transformed from the Cartesian coordinates to symmetry coordinates and then scaled according to the types of internal coordinates using the scheme F_{ij}(scaled) = F_{ij}(ab initio) × $(X_iX_j)^{1/2}$, where X_i and X_j are the scale constants for the diagonal force constants. The scale constants were: 0.89 for SiH-stretching, 0.92 for SiH-bending, 0.93 for SiSi- and SiI-stretching, 0.99 for bending involving the heavy atoms and 1.0 for the SiSi-torsion. The transformed ab initio force field, the ab initio geometry and the atomic masses were then used for the calculation of the vibrational frequencies and PED

Table 3
Calculated and observed fundamental vibrations (cm^{-1}) and PED (contributions $> 10\%$ from diagonal elements only) for *anti* and *gauche* $I_2HSi–SiH_2I$

Vibration		*anti*				*gauche*			
		HW–ECP[a]	SBK–ECP[b]	Observed	PED	HW–ECP[a]	SBK–ECP[b]	Observed	PED
A′	$\nu_1 = \nu$SiH	2152	2145	2160	80(1), 20(2)	2147	2157	2160	95(1)
	$\nu_2 = \nu_s$SiH$_2$	2168	2153	2160	80(2), 20(1)	2163	2161	2160	94(2)
	$\nu_3 = \delta$SiH$_2$	898	914	898	99(3)	905	911	898	99(3)
	$\nu_4 = \gamma$SiH$_2$	771	756	767	99(4)	782	785	779	66(4), 17(5)
	$\nu_5 = \delta$SiSiH	707	700	712	70(5), 27(10)	684	689	677	36(5), 32(4), 12(10)
	$\nu_6 = \nu$SiSi	467	463	463	70(6), 11(7), 12(8)	481	478	479	64(6), 18(15)
	$\nu_7 = \nu$SiI	360	355	353	76(7), 15(8)	354	354	353	92(7)
	$\nu_8 = \nu_s$SiI$_2$	277	283	293	53(8), 20(6), 12(7)	293	297	297	71(8)
	$\nu_9 = \gamma$SiI$_2$	80	83	90	85(9)	66	68	76	58(9)
	$\nu_{10} = \delta$SiI$_2$	182	179	175	37(10), 13(8), 29(11)	115	114	123	61(10), 40(5), 13(15)
	$\nu_{11} = \delta$SiSiI	38	38	–	70(11), 28(5), 28(10)	95	97	102	29(11), 10(8), 31(9)
A″	$\nu_{12} = \nu_{as}$SiH$_2$	2168	2172	2160	100(12)	2170	2180	2160	95(12)
	$\nu_{13} = \delta$HSiI	730	735	736	52(13), 42(17)	735	730	736	52(13), 37(17)
	$\nu_{14} = \tau$SiH$_2$	637	637	635	94(14)	620	626	627	77(14), 14(5)
	$\nu_{15} = \rho$SiH$_2$	471	466	463	84(15), 12(16)	447	446	463	68(15), 13(6), 10(16)
	$\nu_{16} = \nu_{as}$SiI$_2$	392	377	382	93(16), 11(15)	387	385	382	90(16)
	$\nu_{17} = \tau$SiI$_2$	84	81	76	60(17), 59(13), 13(18)	42	39	–	46(17), 75(11), 50(13)
	$\nu_{18} =$ SiSi torsion	19	19	–	89(18)	22	22	–	110(18)

[a] Frequencies from HF/6-31G(d)/HW–ECP(I) force field using refined scale constants as described in the text (cf. Section 3.3.2).
[b] Frequencies from MP2/SBK–ECP force field using the scale constants listed in the text (cf. Section 3.2.2).

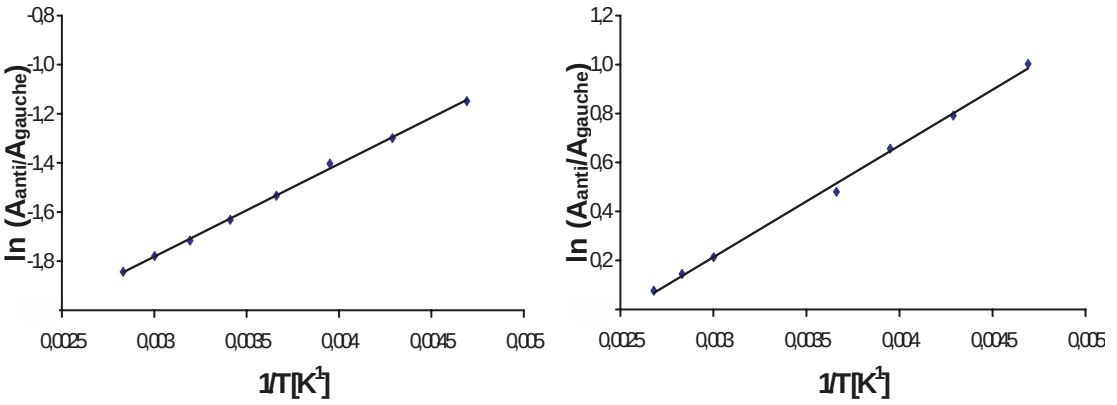

Fig. 7. Van't Hoff plots for the line pairs 90/102 cm^{-1} (left) and 293/297 cm^{-1} (right).

employing the FG-method of Wilson [32]. The program ASYM40 [33,34] was used for this purpose, and the calculated (unscaled) frequencies were initially checked to be identical with the ab initio frequencies. The results of the normal coordinate analysis, including the scaled frequencies and the PEDs are summarized in Table 3 for both the conformers. As can be seen from the PEDs presented in Table 3, almost all of the deformation modes involving the heavy atoms cannot be described accurately within the framework of group vibrations due to extensive vibrational coupling.

3.2.3. Rotational isomerism

In the dihedral angle range of $0 < \phi < 180°$, TIDS possesses two minima on the potential surface for the internal rotation, which correspond to the *anti* and *gauche* conformers. They are illustrated in Fig. 1 with the help of 'semi-Newman' projections. Two line pairs at 293/297 and at 90/102 cm^{-1} were chosen for the determination of the enthalpy difference between the conformers, using Van't Hoff's equation:

$$\ln(A_{anti}/A_{gauche}) = -\Delta H/RT + C \quad (1)$$

with $\Delta H_{A-G} = H_{anti} - H_{gauche}$ and $C = \Delta S/R - \ln(\alpha_{gauche}/\alpha_{anti})$.

By assuming that ΔH, ΔS and the ratio of the scattering coefficients, $\alpha_{gauche}/\alpha_{anti}$, do not depend on temperature, a linear plot of the logarithm of the

Table 4
Molecular parameters and relative energies for 1,1,2-triiododisilane calculated at different levels of ab initio MO and DF theory

Method/basis set:	HF/3-21G		B3PW91/LanL2DZ		B3LYP/3-21G*		HF/6-31G(d)/HW−ECP(I)		MP2/SBK−ECP	
	anti	*gauche*	*anti*	*gauche*	*anti*	*gauche*	*anti*	*gauche*	*anti*	*gauche*
r(Si–Si)	2.364	2.357	2.342	2.338	2.330	2.323	2.350	2.347	2.359	2.353
r(Si–I_3)	2.571	2.585	2.531	2.543	2.465	2.476	2.479	2.489	2.461	2.469
r(Si–I_4)	2.571	2.570	2.531	2.530	2.465	2.462	2.479	2.479	2.461	2.460
r(Si–I_8)	2.574	2.585	2.524	2.535	2.459	2.468	2.476	2.483	2.459	2.466
r(Si–H_2)	1.475	1.472	1.485	1.482	1.485	1.482	1.467	1.464	1.487	1.484
r(Si–$H_{6,7}$)	1.477	1.475	1.484	1.482	1.485	1.484	1.468	1.467	1.486	1.485
∠$SiSiI_3$	109.9	106.8	110.4	107.9	109.3	105.9	111.2	107.9	109.6	107.3
∠$SiSiI_4$	109.9	109.8	110.4	110.6	109.3	110.3	111.2	111.2	109.6	109.9
∠$SiSiI_8$	110.0	108.0	110.9	109.1	110.5	110.1	112.4	110.1	109.6	108.6
∠$SiSiH_2$	111.5	114.1	110.9	112.6	110.8	112.7	109.9	112.9	111.6	113.0
∠ISiI	111.4	110.3	111.6	111.1	113.3	112.5	111.9	111.2	111.9	111.5
∠ISiH (averages)	107.5	107.9	107.6	107.8	108.1	108.4	107.1	107.4	107.9	108.2
ϕ(H_2–Si–Si–I_8)	180.0	52.2	180.0	53.0	180.0	58.7	180.0	51.8	180.0	54.5
ΔE_0 (kcal mol^{-1})	1.3	0	0.9	0	1.1	0	0.9	0	1.1	0

intensity ratio $\ln(A_{anti}/A_{gauche})$ of two bands belonging to the two conformers versus the inverse temperature, will result in a straight line whose slope will be equal to $-\Delta H/R$. Fig. 7 presents the Van't Hoff plots that were obtained for the two line pairs. Integrated intensities were measured by deconvolution of the bands. The two plots give ΔH_{A-G}-values of -3.8 ± 1.0 and -3.1 ± 1.0 kJ mol^{-1} (-0.91 ± 0.24 and -0.74 ± 0.24 kcal mol^{-1}, respectively), with an averaged value of -3.45 ± 1.0 kJ mol^{-1} (-0.82 ± 0.24 kcal mol^{-1}). This value may be compared with the average ab initio result of $\Delta H_{A-G} = +4.6$ kJ mol^{-1} ($+1.1$ kcal mol^{-1}). All the ab initio calculations predicted the *gauche* conformer to be of lower energy, in contrast to the results of the GED and Raman experiments, cf. Table 4. The rather large error of ± 1.0 kJ mol^{-1} (± 0.24 kcal mol^{-1}) in the Raman values is an estimated value larger than the statistical error. It is quite difficult to obtain accurate intensities for bands lying in the ascent of the Rayleigh line (ν_{10}/ν'_{10}), and the accuracy for barely separated bands such as ν_6/ν'_6 is also reduced. Line pairs relating to SiH-deformations (γSiH_2, τSiH_2 or $\delta SiSiH$) were too weak to be of any use in the conformational analysis. Moreover, the SiSi stretching mode (ν_6, ν'_6) is contaminated by ρSiH_2, which makes the ΔH-value obtained thereof about half as large as those obtained from ν_9/ν'_{11} and ν_8/ν'_8.

3.3. Gas electron diffraction analysis

3.3.1. Details of the dynamic model

The GED data were treated by fitting a three-term cosine potential function to the experimental data. The cosine potential

$$V(\phi) = \frac{1}{2}\sum_i V_i[1 - \cos i(180 - \phi)] \qquad (2)$$

with $i = 1$–3 and $\phi = \phi$(HSiSiI), was obtained by using pseudo-conformers, each one representative of a finite displacement of the large-amplitude torsional coordinate, and each given a weight determined by Boltzmann statistics in which the cosine potential $V(\phi)$ appeared as the energy factor [35]. The cosine potential function $V(\phi)$ has the property that $V(180°) = 0$, $V(0°) = V_1 + V_3$, and $V(60°) = 3/4(V_1 + V_2)$. By using the pseudo-conformers at 30° intervals from *syn* (0°) to *anti* (180°), comprising a total of seven pseudo-conformers, refined values for V_1, V_2 and V_3 were obtained simultaneously. The experimental torsional potential curve for the rotation around the Si–Si bond could be calculated from these values. The C_s forms (0 and 180°) were given half the statistical weight of the C_1 forms (30° through 150°) in the Boltzmann calculations due to multiplicity considerations. We will give details about how the results were derived from the cosine potential function in another section below.

3.3.2. Refinements and normal coordinate calculations

From the experimental RD curve and from the theoretical calculation results, trial values for bond distances and bond angles were obtained for TIDS. Refinements of the molecular structure based on the GED data were made by the least-squares method [36], adjusting a theoretical $sI_m(s)$ curve simultaneously to the 11 experimental intensity curves, one from each of the photographic plates, using a unit weight matrix. The structures were converted from the geometrically consistent r_α to the r_a-type, required by the formula for the theoretically scattered intensities ($r_a = r_g - \ell^2/r = r_\alpha - \ell^2/r + K_T + \delta r$) [37,38], by using the values of the centrifugal distortion constants (δr), perpendicular amplitude corrections (K_T) and root-mean-square amplitudes of vibration (ℓ) calculated at the average temperature of the experiment, 325 K. These vibrational quantities were estimated from the ab initio Cartesian force fields (HF/6-31G(d)/HW–ECP(I)) using NCA and ASYM40, as previously described in Section 3.2. A set of scale factors for the non-redundant set of symmetry force constants for each conformer (six scale factors for the C_s conformer, five for the C_1 conformer) was then refined to fit the observed vibrational wavenumbers presented in Table 3. Particularly, the scale constants for the Si–I stretching modes became 1.06 ($\sigma = 0.06$; *anti*) and 1.01 ($\sigma = 0.03$; *gauche*), the Si–Si stretching mode scale constants became 0.81 ($\sigma = 0.05$; *anti*) and 0.85 ($\sigma = 0.04$; *gauche*). The bending modes scale constants all became ca. 0.80–0.85 from this procedure. The resulting SQM force fields were used to calculate the vibrational amplitudes and corrections previously described. The calculated wavenumbers from the SQM force fields agreed with the experimental

Table 5
Structural and potential parameters for the torsional vibrational average of 1,1,2-triiododisilane, along with ab initio calculations for the structures of the *anti* and *gauche* conformers (Distances (r) and amplitudes (ℓ) are in angstroms (Å), angles ($\angle$) in degrees. Parenthesized values are 2σ, where σ includes estimates of uncertainty in voltage/nozzle heights and of correlation in the experimental data. The GED parameter values are calculated according to Eq. (3)

	Gas electron diffraction				B3LYP/3-21G*	
	$r_\alpha^{aver}, \angle_\alpha$	r_g^{aver}	ℓ_{exp}	ℓ_{calc}	*anti*	*gauche*
r(Si–Si)	2.322(12)	2.329	0.049(9)	0.059	2.330	2.323
r(Si–I)	2.438(3)	2.449	0.046(9)	0.055	2.463	2.469
r(Si–H)	[1.507]	[1.527]		0.090	1.485	1.483
Δ_1(Si–I)[a]	[−0.0067]				[−0.0067]	[−0.0072]
Δ_2(Si–H)[b]	[0.0001]				[0.0001]	[−0.0015]
$\angle$SiSiI$_{3,4}$	109.2(4)				109.3	105.9/110.3
$\angle$SiSiI$_8$	111.2(4)				110.5	110.1
$\angle$SiSiH	[110.1]				109.8	111.0
Δ_3(SiSiI)[c]	[1.2377]				[1.2377]	[4.1850]
Δ_4(SiSiH)[d]	[1.5299]				[1.5299]	[3.4378]
$\angle$ISiI[e]	110.5(4)				113.3	112.5
$\angle$ISiH[e]	109.0(2)				108.1	108.4
V_1 (kcal mol^{-1})	0.7 ± 1.1					
V_2 (kcal mol^{-1})	−0.4 ± 1.0					
V_3 (kcal mol^{-1})	0.4 ± 0.6					
ϕ_G	79.8°[f]				–	58.7°

[a] Δ[r(Si–I$_8$) − r(Si–I$_3$)]; *anti* value.
[b] Δ[r(Si–H$_2$) − r(Si–H$_{6,7}$)]; *anti* value.
[c] Δ[$\angle$SiSiI$_8$ − $\angle$SiSiI$_3$]; *anti* value.

ones within an average of $\pm 7\,cm^{-1}$ margin, and they are listed in Table 3 along with the MP2/SBK–ECP and experimental wavenumbers. The use of a dynamic model in the GED analysis enforces the removal of the contribution from the large-amplitude torsional symmetry coordinate to the harmonic NCA calculation [35], and the corresponding diagonal internal force constants were, therefore, set to intentionally high values. In this way, reasonable values for the frame amplitudes and perpendicular corrections used in the GED refinements were obtained. The symmetrized SQM force fields obtained for the minimum-energy *anti* and *gauche* geometries (using the HW–ECP(I) ab initio results) were used in the calculation of similar frame amplitude values for all pseudo-conformers comprised by the dynamic model, by using the obtained B3LYP/3-21G* optimized geometries.

3.3.3. The GED molecular parameters

The geometry of each of the conformers can be described by a set of independent parameters, which were fitted to the experimental data. In our refinements these parameters were chosen as ('⟨ ⟩' denotes average value): r(Si–Si), r(⟨Si–I⟩), r(⟨Si–H⟩), $\angle$(⟨SiSiH⟩), $\angle$(⟨SiSiI⟩), P(ISiI) (projection angle; the angle between the two Si–I bonds projected on a plane perpendicular to the Si–Si –bond), P(HSiI) (similar projection angle), the torsional angle parameter ϕ(HSiSiI) (in increments of 30°), along with the three potential constants V_1, V_2, V_3 and several difference parameters held at constant values (cf. text below Table 5). Ab initio constraints were incorporated as described earlier. The r(Si–H) parameter value could not be refined and was held constant in the least squares refinements, and the r_α value used was calculated from the assumed r_e ab initio value (B3LYP/3-21G*) by using the anharmonicity constant

Table 6
Correlation matrix (× 100) for the refined parameters of 1,1,2-triiododisilane

Parameter:	σ_{LS}[a]	r_1	r_2	$\angle_3$	V_1	V_2	V_3	ℓ_1	ℓ_2	ℓ_3
Si–Si	0.4	100								
Si–I	0.08	−41	100							
SiSiI	12.8	−4	8	100						
V_1	40.1	−22	33	−27	100					
V_2	37.0	28	−14	5	−83	100				
V_3	19.8	−8	25	−34	77	−53	100			
ℓ(Si–Si)	0.3	74	−40	−1	−13	22	−6	100		
ℓ(I·I)	0.2	16	6	−14	28	−23	20	30	100	
ℓ(Si··I)	0.8	17	−18	59	−32	36	−34	35	−23	100

[a] Standard deviations (× 100) from least-squares refinement. Distances (r) and amplitudes (ℓ) are in ångstrøms; angles ($\angle$) are in degrees.

$a_3 = 2.0$ Å^{-1} [39] in the usual formula $r_\alpha = r_e + 3a_3\ell^2/2$. The r_g value is then $r_g = r_e + 3a_3\ell^2/2 + K$, where K is the perpendicular amplitude correction. The vibrational properties of the molecule were specified by 28 amplitude parameters for each pseudo-conformer, corresponding to the number of interatomic distances in the molecule, making a total of 196 weighted distances included in the dynamic theoretical model. Many, but not all, of the amplitudes could successfully be refined. The amplitudes were refined together in groups, depending on the interatomic distances. The amplitudes, which could not be refined, were kept constant at the values calculated from the NCA. In the final refinement three geometrical parameters, three amplitude parameters and three potential constants (V_i) were refined simultaneously. The results of this refinement are given in Table 5 where the corresponding geometrical values from the B3LYP/3-21G* ab initio calculations are also given. The correlation matrix for the refined parameters is given in Table 6. In Table 7 are shown the experimentally obtained energy values from the three-term potential function together with the corresponding results from the ab initio calculations, the Raman values, and also available (non-published) molecular-mechanics (MM) calculations [40]. In Table 8 the results for TIDS are compared with the previous GED results for 1,2-diiododisilane [8], 1,1,2,2-tetraiododisilane [8], 1,1,2,2-tetrabromodisilane [41], and the 1,1,2,2-tetrachlorodisilane [1]. The theoretical intensity curve for the final model is shown in Fig. 2 together with average experimental and difference curves. The corresponding RD curves along with the difference curve are shown in Fig. 3.

3.3.4. Deriving results from the cosine potential model

It might be useful here to state some formulas derived from using the cosine potential function. When dealing with a dynamic model in the GED least-squares refinements, the question opens whether an "equilibrium" or a torsional vibrational averaged structure is of more significance. The refinements of the three potential constants V_i ($i = 1–3$) in the present case gave quite low energy barriers to torsional motion (0.1–0.9 kcal mol^{-1}). This should imply that the GED experimental molecular structure is better represented by weighted contributions from some or all of the pseudo-conformers. This favours presenting a torsional vibrational average molecular structure for TIDS, where the set of average structural parameters $R_\alpha^{aver}(i)$ (representing the complete r_α structure) is calculated by using the Boltzmann mole fractions α_N for each pseudo-conformer N:

$$R_\alpha^{\text{aver}}(i) = \sum_{N=1}^{7} R_{\alpha,N}(i) \times \alpha_N \tag{3}$$

running over all i's that make up the set of (independent) structural parameters (bond distances and bond angles, including projection angles). The torsional vibrational average r_g structure and the set of torsional average vibrational amplitudes ℓ_{ij} may be obtained in a similar fashion. As the parameter V_2 in the cosine potential function is refined to be non-zero, the only way to obtain the exact (numerical) minimum corresponding to the *gauche* torsional angle would be by differentiating Eq. (2) with respect to the variable ϕ, and solving the equation $\partial V(\phi)/\partial\phi = 0$. The first

Table 7
Torsional potential values and pseudo-conformational distributions of 1,1,2-triiododisilane as obtained from various theoretical and physical methods (Energy values in kcal mol^{-1}. All distributions estimated by using standard Boltzmann statistics, calculated at $T = 325$ K)

Pseudo-form	GED energies[a]	GED % distribution	B3LYP energies[b]	B3LYP % distribution	Molecular mechanics energies[c]	MM. % distribution	Exp. Raman energies	Raman % distribution
0	1.06	2.5	1.6	2.3	2.9	0.9	–	–
30	0.73	8.3	0.6	22.6	2.5	3.3	–	–
60	0.25	17.7	0.0	55.6	2.1	6.2	0.82(24)	36.0
90	0.17	20.1	1.1	10.0	3.6	0.6	–	–
120	0.27	17.3	2.4	1.3	4.1	0.3	–	–
150	0.14	21.1	1.9	2.9	1.9	8.5	–	–
180	0.0	13.0	1.1	5.3	0.0	80.2	0.0	64.0

[a] Values obtained from the cosine potential function described in the text. An estimate of the amount of the vibrational average *anti* conformer is obtained by summing the pseudo-conformational contributions 120–180. This gives a value of 51.4% for the *anti* conformer, and a more realistic energy difference between the *anti* and *gauche* of 0.63 kcal mol^{-1} in favour of the *anti* form (including vibrational/rotational entropy differences).

[b] Values from the B3LYP/3-21G* calculations.

[c] Values obtained by molecular-mechanics (MM) calculations from Ref. [40].

Table 8
Comparison of results from GED investigations (r_g, $\angle_\alpha$) and MW (r_0) of six closely related disilanes (X = Cl, Br, I) (Distances are in angstroms (Å), angles ($\angle_\alpha$) in degrees)

Parameter:	$IH_2Si–SiH_2I$	$I_2HSi–SiHI_2$	$Br_2HSi–SiHBr_2$	$Cl_2HSi–SiHCl_2$[a]	$I_2HSi–SiH_2I$	$IH_2Si–SiH_3$ (MW)
r(Si–Si)	2.380(34)	2.389(37)	2.350(19)	2.310(8)	2.329(12)	2.336(9)
r(Si–X)	2.429(13)	2.440(9)	2.206(5)	2.039(2)	2.449(3)	2.440(9)
r(Si–H)	1.510(25)	1.50[b]	1.490[b]	1.511[b]	1.527[b]	1.485(9)
∠SiSiX	107.5(12)	107.2(10)	107.1(12)	108.9(4)	109.9(4)	106.7(3)
∠XSiX	–	111.4(6)	110.1(16)	109.7(3)	110.5(4)	
∠SiSiH	111.9(157)	111.9[b]	108.6[b]	111.5[b]	110.1[b]	111.5(18)
∠XSiH	107.9(170)	109.6(8)	–	108.9(5)	109.0(2)	
$r(X\cdots X)_{anti}$	5.97	5.97	5.54	5.26	6.01	
$r(X\cdots X)_{gauche}$	4.41	4.45	4.19	4.11	4.57	
ϕ(*anti*)[c]	180	180	180	180	180	
ϕ(*gauche*)[c]	58(31)	61(27)	60[b]	60[d]	80[e]	
$\alpha \times 100$ (*gauche*)[f]	76(16)	60(29)	50(20)	80	49	
Reference	[8]	[8]	[41]	[1]	This work.	[9]

[a] *Gauche* values.
[b] Assumed value.
[c] Torsional angles. For *anti* a C_{2h} (C_s for $I_2HSi–SiH_2I$) symmetry was used, with torsional angles of exactly 180°.
[d] Studied by using a dynamic model [1].
[e] Calculated from Eq. (5) using the refined V_1, V_2, V_3 parameters, as explained in the text.
[f] Estimated percentage of the *gauche* conformer observed in the gas phase.

derivative of Eq. (2), $V'(\phi) = \partial V(\phi)/\partial\phi$, is given by

$$V'(\phi) = -\frac{1}{2}\sum_i V_i i \sin[i(180 - \phi)] \quad (4)$$

with $i = 1–3$ in the case of TIDS. Solving the equation $\partial V(\phi)/\partial\phi = 0$ then gives four extremal values (two minima and two maxima), of which the more interesting *gauche* torsional angle ϕ_G may be written as

$$\phi_G = 180 - \cos^{-1}\left(\frac{-4V_2 - \sqrt{16V_2^2 - 48V_3(V_1 - 3V_3)}}{24V_3}\right) \quad (5)$$

with $V_3 \neq 0$. Eq. (5) gives the relation between the *gauche* minimum torsional angle and the obtained potential parameters V_i, $i = 1–3$. These formulas (3)–(5) have been used in the present work for obtaining the most accurate results possible from the dynamic GED model (cf. Tables 5, 7 and 8).

4. Discussion

In this work, we have presented the experimental and theoretical results on geometries, the torsional potential function and the normal-mode vibrational frequencies for TIDS. Early in the GED study it was possible to fit the experimental data by using only a two-conformer model (*anti* and *gauche*). However, the calculated shrinkage correction values were all too high, and we decided to deal with the apparent large-amplitude torsional motion by using the cosine potential function in Eq. (2). Perhaps the single most outstanding 'insight' that we have obtained using the GED and the IR/Raman spectroscopic data, is a glaring discrepancy with the ab initio MO and DFT methods regarding conformational stability. In Table 4 we have assembled the ab initio calculations, including the conformational energy differences corrected for ZPE's. In every case the result was that the *gauche* conformer ought to be the more stable form, by an average 1.1 kcal mol^{-1}. This was in clear contrast with both the GED and the Raman energy results, which gave the *anti* conformer the lower energy, by an estimated 0.63 and 0.82 kcal mol^{-1}, respectively (cf. Table 7).

The potential parameters V_1, V_2, V_3 obtained from the GED least-squares refinement (cf. Table 5) were $V_1 = 0.7 \pm 1.1$, $V_2 = -0.4 \pm 1.0$ and $V_3 = 0.4 \pm 0.6$ kcal mol^{-1}. These parameters all converged simultaneously in the refinement, which in our experience [1,4,5] is quite unusual when using experimental GED data. Also, the obtained parameter values made the torsional potential rather "flat", with quite low barriers to torsional motion (0.1–0.9 kcal mol^{-1}). Assuming this to be an appropriate potential function for the molecule, the pseudo-conformational distribution was proportioned quite evenly, as seen from Table 7. Even the eclipsed forms 120 and 0 were calculated to contribute ca. 17 and 3% to the scattering intensity, respectively. Related to this, it became important to use ab initio geometries and calculate constraints between the pseudo-conformers to be incorporated into the GED model. For this purpose we preferred using the B3LYP/3-21G* method. It may be seen from Table 4 that most of the ab initio methods overestimated the *r*(Si–Si) and *r*(Si–I) bond distances significantly. The method performing the worst was HF/3-21G, which was not surprising, but also the B3PW91/LanL2DZ method performed poorly regarding the *r*(Si–I) bond distances, giving values above 2.53 Å. When compared to the experimental GED values in Table 5, the B3LYP/3-21G* method seems to perform quite well, and more so than any other method listed in Table 4. The *r*(Si–Si) bond distance was especially well reproduced by this method, giving values of 2.330 Å (*anti*) and 2.323 Å (*gauche*), compared to the weighted average value of 2.322(12) Å (r_α) obtained from the GED data.

The GED values listed in Table 5 are the torsional vibrational averages calculated according to Eq. (3). The torsional angle (ϕ_G) for the *gauche* conformer (in the vibrational average sense) in Table 5 was calculated using Eq. (5) employing the estimated potential parameters V_i ($i = 1$–3). Obviously, the calculated ϕ_G from Eq. (5) seemed too high relative to the B3LYP/3-21G* value of only 58.7°, and with the other ab initio calculations ranging from ca. 52–55°, cf. Table 4. However, the quite large standard errors in the potential parameters ($2\sigma = 0.6$–1.1 kcal mol^{-1}) made it difficult to decide if the difference was significant. We might add that when the *gauche* torsional angle was refined explicitly using the two-conformer model mentioned previously, the obtained value was $\phi_G = 72 \pm 12°$ (2σ), i.e. insignificantly different from the value $\phi_G \approx 80°$ obtained using Eq. (5).

The torsional barrier heights obtained from the B3LYP/3-21G* calculations were much higher than the ones obtained from Eq. (2), using the refined potential parameters. The MM barrier values [40] were also relatively large, and the high relative energy values for the pseudo-conformers (1.9–4.1 kcal mol^{-1}) made the pseudo-conformational distribution much more uneven than in the GED/B3LYP results, ending up with a heavy list towards the *anti* form (ca. 80%), cf. Table 7. It should be noted, however, that MM was the only theoretical method giving *anti* the lower energy, in agreement with GED and Raman experiments. The torsional barrier heights may be summarized in the order MM/B3LYP/GED: for the barrier *gauche* → *gauche* (kcal mol^{-1}), 0.8/1.6/0.9; for the barrier *gauche* → *anti*, 2.0/2.4/0.1; for the barrier *anti* → *gauche*, 4.1/1.3/0.3. We could not find much consistency in these numbers, neither between the available theoretical data, nor between the experiment and theory. With such low experimental barrier heights (0.1–0.9 kcal mol^{-1}), the physical meaning of the obtained potential parameter- and energy results is easily questioned, and in light of other experimental and theoretical works [6,7] such questions are probably justified also in the case of TIDS.

The experimental and theoretical RD-curves for TIDS are shown in Fig. 3. The conformational dependent part is solely determined by the range of (I···I) non-bonded interactions. Even at interatomic distances as high as 5–6 Å, the contribution to the scattering is significant. Using a dynamic model like in the present work, the distribution of the $(I\cdots I)_{4-8}$ and $(I\cdots I)_{3-8}$ torsion-dependent interactions may be seen from the bars marked on the theoretical curve in Fig. 3 (cf. Fig. 1 for atom numbering). The range for the $(I\cdots I)_{4-8}$ interactions is 4.24–5.57 Å (120 and 0 forms, respectively), and the range for the $(I\cdots I)_{3-8}$ interactions is 4.57–6.01 Å (180 and 60 form, where this interaction is of an *anti* type, respectively). We may also list some vibrational amplitudes for important non-bonded distances (Å): For the *anti* conformer (exp./theo.): $\mathcal{l}(I_3\cdots I_4)$, 0.120(7)/0.126; $\mathcal{l}(Si\cdots I)$, 0.179(24)/0.138; $\mathcal{l}(I\cdots I)_{gauche}$, 0.254(11)/0.261. For the gauche conformer (exp./theo.): $\mathcal{l}(I_3\cdots I_4)$,

0.119(7)/0.125; ℓ(Si···I): 0.192(24)/0.149; $\ell(I\cdots I)_{gauche}$, 0.262(11)/0.268; $\ell(I\cdots I)_{anti}$, (*not refined*)/0.129. Given the satisfying agreement between experimental and theoretical RD-curves, we felt that the obtained potential parameters should be quite reliable within the error limits given (overall 'quality of fit' factor, $R = 0.154$).

Table 8 gives structural data on some related disilane molecules, mostly studied by GED (r_g), including the iododisilane studied by Durig et al. [9] using MW spectroscopy (r_0). For TIDS the values listed are weighted according to Eq. (3), but its *r*(Si–Si) bond distance value is not significantly different from the one in iododisilane (2.329(12) and 2.336(9) Å, respectively), and is indeed very similar to the value found in hexaiododisilane (2.323(4) Å; solid state) by X-ray diffraction [10]. The *r*(Si–I) values are also quite similar within the standard errors given. The value for *r*(Si–Si) found in *gauche* 1,1,2,2-tetrachlorodisilane [1] was rather low (2.310(8) Å), but this value seems reasonable when compared to the values in $H_3Si–SiH_3$ (2.332(3) Å), $F_3Si–SiF_3$ (2.319(6) Å) and $Cl_3Si–SiCl_3$ (2.320(30) Å), as tabulated by Oberhammer [6]. The higher *r*(Si–Si) values of 2.380(34) and 2.389(37) Å found in 1,2-diiododisilane and 1,1,2,2-tetraiododisilane [8], respectively, were even higher than the "worst-case" ab initio results for TIDS shown in Table 4 (ca. 2.360 Å). Even in hexamethyldisilane ($(CH_3)_3Si–Si(CH_3)_3$), the experimental *r*(Si–Si) bond distance was not found higher than 2.342(9) Å [42]. Thus, the bond distance values observed in the earlier two iododisilanes [8] may seem a bit too large, although the experimental standard errors have to be taken into consideration.

In conclusion, the new structural results for TIDS fit the earlier investigations on similar molecules well, and the real challenge lies in obtaining more reliable conformational- and torsional barrier energy differences. Future disilane investigations with one or more of the heavier halogens (Br, I) will hopefully bring further insight into the conformational properties of these compounds.

Acknowledgements

We are very grateful to Hans Vidar Volden and Snefrid Gundersen at the University of Oslo for their help in the electron-diffraction data collection. This work has received support from The Research Council of Norway (Program for Supercomputing) through grants of computing time.

References

[1] T.H. Johansen, K. Hagen, R. Stølevik, J. Mol. Struct. 485–486 (1999) 121–133.
[2] M. Ernst, K. Schenzel, A. Jähn, W. Köll, K. Hassler, J. Raman Spectrosc. 28 (1997) 589.
[3] P.v.R. Schleyer, M. Kaupp, F. Hampel, M. Bremer, K. Mislow, J. Am. Chem. Soc. 114 (1992) 6791.
[4] T.H. Johansen, K. Hagen, K. Hassler, A. Richardson, U. Pätzold, R. Stølevik, J. Phys. Chem. A 101 (1997) 9641.
[5] T.H. Johansen, K. Hagen, K. Hassler, A.D. Richardson, U. Pätzold, R. Stølevik, J. Phys. Chem. A (1999) submitted for publication.
[6] H. Oberhammer, J. Mol. Struct. 31 (1976) 237.
[7] S.G. Cho, O.K. Rim, G. Park, J. Comput. Chem. 12 (1997) 1523.
[8] E. Røhmen, K. Hagen, R. Stølevik, K. Hassler, M. Pöschl, J. Mol. Struct. 244 (1991) 41.
[9] J.R. Durig, J.S. Church, Y.S. Li, Inorg. Chem. 21 (1982) 35.
[10] M. Jansen, B. Friede, Acta Cryst. C52 (1996) 1333.
[11] K. Hassler, W. Köll, K. Schenzel, J. Mol. Struct. 348 (1995) 353.
[12] W.R. Wadt, P.J. Hay, J. Chem. Phys. 82 (1985) 284.
[13] M.J. Frisch, G.W. Trucks, H.B. Schlegel, P.M.W. Gill, B.G. Johnson, M.A. Robb, J.R. Cheeseman, T. Keith, G.A. Petersson, J.A. Montgomery, K. Raghavachari, M.A. Al-Laham, V.G. Zakrzewski, J.V. Ortiz, J.B. Foresman, J. Cioslowski, B.B. Stefanov, A. Nanayakkara, M. Challacombe, C.Y. Peng, P.Y. Ayala, W. Chen, M.W. Wong, J.L. Andres, E.S. Replogle, R. Gomperts, R.L. Martin, D.J. Fox, J.S. Binkley, D.J. Defrees, J. Baker, J.P. Stewart, M. Head-Gordon, C. Gonzalez, J.A. Pople, Gaussian 94, Revision D.4, Gaussian, Inc., Pittsburgh, PA, 1995.
[14] W. Stephens, H. Basch, J. Krauss, J. Chem. Phys. 81 (1984) 6026.
[15] W. Stephens, J. Krauss, H. Basch, P.G. Jasien, Can, J. Chem. 70 (1992) 612.
[16] M.W. Schmidt, K.K. Baldridge, J.A. Boatz, S.T. Elbert, M.S. Gordon, J.H. Jensen, S. Koseki, N. Matsunaga, K.A. Nguyen, S.J. Su, T.L. Windus, M. Dupuis, J.A. Montgomery, GAMESS version 1994, J. Comput. Chem. 14 (1993) 1347.
[17] M.J. Frisch, A.E. Frisch, J.B. Foresman, Gaussian 94 User's Reference, Gaussian, Inc., 1994-1995, Carnegie Office Park, Pittsburgh, PA 15106 USA, p. 24.
[18] A.D. Becke, J. Chem. Phys. 98 (1993) 5648.
[19] W. Köll, Dissertation, Technical University Graz, 1995.
[20] W. Zeil, J. Haase, L. Wegmann, Z. Instrumentenkd. 74 (1966) 84.

[21] S. Gundersen, T.G. Strand, H.V. Volden, J. Mol. Struct. 346 (1995) 121.
[22] S. Gundersen, T.G. Strand, J. Appl. Cryst. 29 (1996) 638.
[23] K. Hagen, K. Hedberg, J. Am. Chem. Soc. 95 (1973) 1003.
[24] B. Andersen, H.M. Seip, T.G. Strand, R. Stølevik, Acta Chem, Scand. 23 (1969) 3224.
[25] G. Gundersen, K. Hedberg, J. Chem. Phys. 51 (1969) 2500.
[26] L. Hedberg, Abstracts of Papers, in: 5th Austin Symposium on Gas-phase Molecular Structure, Austin, TX, March 1974, p. 37.
[27] A.W. Ross, M. Fink, R. Hilderbrandt, International Tables of Crystallography, 4, Kluwer Academic, Dordrecht, 1992, p. 245.
[28] D. Van Hemelrijk, L. Van den Enden, H.J. Geise, H.L. Sellers, L. Schäfer, J. Am. Chem. Soc. 102 (1980) 2189.
[29] L. Schäfer, J.D. Ewbank, K. Siam, N. Chiu, H.L. Sellers, in: I. Hargittai, M. Hargittai (Eds.), Stereochemical Applications of Gas-Phase Electron Diffraction, VCH Publishers, New York, 1988, pp. 301.
[30] V.J. Klimkowski, J.D. Ewbank, C. Van Alsenoy, J.N. Scardale, L. Schäfer, J. Am. Chem. Soc. 104 (1982) 1476.
[31] K. Hassler, W. Köll, M. Ernst, Spectrochim. Acta 53A (1997) 213.
[32] E.B. Wilson Jr., J.C. Decius, P.C. Cross, Molecular Vibrations, McGraw-Hill, New York, 1955.
[33] L. Hedberg, I.M. Mills, J. Mol. Spectrosc. (ASYM20) 160 (1993) 117.
[34] L. Hedberg, Abstracts, in: 15th Austin Symposium on Molecular Structure, Austin, TX, March 1994.
[35] K. Hedberg, in: J. Laane, M. Dakkouri, B. van der Veken, H. Oberhammer (Eds.), Structures and Conformations of Non-Rigid Molecules, Kluwer Academic, Netherlands, 1993, vol. 410, pp. 423–445.
[36] K. Hedberg, M. Iwasaki, Acta Crystallogr. 17 (1964) 529.
[37] L.S. Bartell, J. Chem. Phys. 38 (1963) 1827.
[38] K. Kuchitsu, Y. Morino, Bull. Chem. Soc. Jpn. 38 (1965) 841.
[39] K. Kuchitsu, M. Nakata, S. Yamamoto, in: I. Hargittai, M. Hargittai (Eds.), Stereochemical Applications of Gas-Phase Electron Diffraction, Part A, VCH Publishers, New York, 1988, pp. 235–236 Table 7.2).
[40] K.H. Wold, Cand. Scient. thesis, University of Trondheim, AVH, 1994.
[41] H. Thomassen, K. Hagen, R. Stølevik, K. Hassler, J. Mol. Struct. 147 (1986) 331.
[42] B. Beagley, J.J. Monaghan, T.G. Hewitt, J. Mol. Struct. 8 (1971) 401.